ESC European Society of Cardiology

Cardiovascular Research (2020) **116**, 605–618
doi:10.1093/cvr/cvz182

HAND1 loss-of-function within the embryonic myocardium reveals survivable congenital cardiac defects and adult heart failure

Beth A. Firulli[1], Rajani M. George [1], Jade Harkin [1], Kevin P. Toolan [1], Hongyu Gao[2], Yunlong Liu[2], Wenjun Zhang[1], Loren J. Field [1], Ying Liu[1], Weinian Shou [1], Ronald Mark Payne [1], Michael Rubart-von der Lohe[1], and Anthony B. Firulli [1]*

[1]Department of Pediatrics, Anatomy, Biochemistry, and Medical and Molecular Genetics, Herman B Wells Center for Pediatric Research, Indiana University School of Medicine, 1044 W. Walnut St, Indianapolis, IN 46202-5225, USA; and [2]Department of and Medical and Molecular Genetics, Center for Computational Biology and Bioinformatics, Indiana University School of Medicine, 975 West Walnut Street, Indianapolis, IN 46202-5225, USA

Received 22 January 2019; revised 14 May 2019; editorial decision 2 July 2019; accepted 5 July 2019; online publish-ahead-of-print 9 July 2019

Time for primary review: 17 days

Aims To examine the role of the basic Helix-loop-Helix (bHLH) transcription factor HAND1 in embryonic and adult myocardium.

Methods and results *Hand1* is expressed within the cardiomyocytes of the left ventricle (LV) and myocardial cuff between embryonic days (E) 9.5–13.5. Hand gene dosage plays an important role in ventricular morphology and the contribution of *Hand1* to congenital heart defects requires further interrogation. Conditional ablation of *Hand1* was carried out using either Nkx2.5 knockin Cre (*Nkx2.5*^{Cre}) or α-myosin heavy chain Cre (*αMhc-Cre*) driver. Interrogation of transcriptome data via ingenuity pathway analysis reveals several gene regulatory pathways disrupted including translation and cardiac hypertrophy-related pathways. Embryo and adult hearts were subjected to histological, functional, and molecular analyses. Myocardial deletion of *Hand1* results in morphological defects that include cardiac conduction system defects, survivable interventricular septal defects, and abnormal LV papillary muscles (PMs). Resulting *Hand1* conditional mutants are born at Mendelian frequencies; but the morphological alterations acquired during cardiac development result in, the mice developing diastolic heart failure.

Conclusion Collectively, these data reveal that *HAND1* contributes to the morphogenic patterning and maturation of cardiomyocytes during embryogenesis and although survivable, indicates a role for Hand1 within the developing conduction system and PM development.

Keywords *HAND1* • Mitral arcade • Heart failure with preserved ejection fraction • Right bundle branch block • Transcription • Cardiac development

1. Introduction

During the process of cardiogenesis, a co-ordination of cell specification, migration and differentiation of cardiomyocytes, endocardial cells, neural crest, and epicardium co-ordinate the morphogenetic patterning of the heart from a simple linear tube to a four-chambered structure with defined pulmonary and systemic circulations.[1–8] The orchestration of cardiac morphogenesis lies within the gene regulatory networks that determine these cell types. When these gene regulatory networks break down, the result is often congenital heart defects (CHDs), which are observed in almost one percent of live births.[9–12] CHDs that result in morphological alterations within the left side of the heart exhibit the poorest clinical outcomes[13] and the identification of the genes causative of left-sided CHDs has been a priority in defining mechanisms of development. Transcription factors that include TBX5,[14,15] NKX2.5,[16] and GATA4[17,18] are associated with the development of CHDs; however, the incidence of CHDs that are linked to defined genetic causes are small in comparison to the total number of cases presented.[19]

The bHLH transcription factor HAND1 uniquely marks the cardiomyocytes of the left ventricle (LV) as well as a ring of second heart field

* Corresponding author. Tel: 317-278-5814; fax: 317-278-9298, E-mail: tfirulli@iu.edu

cardiomyocytes that directly contacts the cardiac outflow tract called the myocardial cuff; however, the necessity of *Hand1* in extraembryonic tissues is thought to preclude the inheritance of HAND1 loss-of-function mutations due to embryonic lethality.[20–22] Conditional *Hand1* ablations within the myocardium reveals a role for *Hand1* in the formation of the intraventricular septum (IVS) and disruption of valvulogenesis resulting in neonatal death.[23] The data within this study confirms and expands these embryonic phenotypes; however, our cardiomyocyte model of Hand1 knockouts survives in larger numbers. More recently, the idea of somatic *HAND1* mutations has been proposed and indeed *HAND1* mutations in patient tissue samples are reported[24–26] as well as evidence of inherited *HAND1* mutations[27,28]; however, testing the identified *HAND1* mutant in mice did not reproduce expected phenotypes.[29] LV-specific deletion of *Hand1* and *Hand2* in mice results in mice that are viable but exhibit aberrant trabeculation and thickened compact zone myocardium.[30] In this study, we conditionally delete *Hand1* from embryonic cardiomyocytes and perform E11.5 transcriptome analysis on isolated ventricles. Data reveal expression changes in a number of gene regulatory pathways, which are often observed as being dysregulated in adult cardiac failure. Next, we allowed cardiomyocyte conditional knockout (*H1CKO*) mice to go to birth. Results show *H1CKOs* are born at Mendelian frequencies, are viable, fertile, and survive into adulthood; however, *H1*CKO mice have cardiac conduction defects, develop cardiac hypertrophy, heart dilation, and heart failure with preserved ejection fraction (HFpEF) resulting in death.

2. Methods

2.1 Mouse strains and genotyping

The *Hand1* conditional ($Hand1^{f/f}$) mice[23] were out crossed and maintained on a mixed C57b/6; 129SV; NIH-SWISS background. Genotyping was performed by Southern blot as described previously[21,22,31,32] or with allelic-specific primers H1 Sense 5'- GGG AGG GAC ATA GGC GGG CGG GTT TT-3' and H1 Antisense 5'-GGG GTG CGG CGG GTG TGA GTG GTG-3' using PCR conditions of 94°C 2 min, 63°C 1 min, 72°C 1 min for 30 cycles, and 72°C 5 min. B6.129S4-*Gt(ROSA)26Sortm1Sor/J* (*ROSA26R-β-gal* homozygous; $R26R^{lacZ}$) mice were genotyped using a probe located 5' of the Stop-Flox (and provided by Dr Phillippe Soriano). $Hand1^{f/f}$ alleles were bred onto a $R26R^{lacZ}$ homozygous background and females of this genotype were crossed to either the *Nkx2.5* knockin *Cre* ($Nkx2.5^{Cre}$)[33] or *α-myosin heavy chain Cre* (*αMhc-Cre*).[34] $Nkx2.5^{Cre}$; $Hand1^{f/f}$; $R26R^{lacZ}$ or *αMhc-Cre*; $Hand1^{f/f}$; $R26R^{lacZ}$ mice were bred for all adult studies. Cre mice were genotyped for the Cre allele either via Southern blot or PCR using the primers Cre(F) 5'- ATTCTCCCACCGTCAGTACG-3' and Cre(R) 5'- CGTTT TCTGAGCATACCTGGA-3' as described.[30]

2.1.1 Ethics statement

No anaesthetic/analgesic agents were used. Euthanasia was performed using CO_2 gas in a closed chamber followed by cervical dislocation. All experiments were performed conforming to the NIH guidelines following the Indiana University IACUC animal protocol 11326.

2.2 RNA capture followed by sequencing (RNA Seq)

Poly-A RNA was processed for library construction by Cofactor Genomics (http://cofactorgenomics.com, Saint Louis, MO, USA) from both right ventricle (RV) and LVs of 2–3 representatives of the following genotypes at E11.5: ($Nkx2.5^{Cre/+}$;$Hand1^{f/f}$), ($Nkx2.5^{+/+}$; $Hand1^{f/f}$), and ($Nkx2.5^{Cre/+}$;$Hand1^{+/+}$; $N = 6$/genotype). Poly-A selected RNA was sheared to appropriate size for cDNA synthesis. Double-stranded cDNA was end-repaired and A-tailed for adaptor ligation. Indexed adaptors were ligated to sample DNA, and the adaptor-ligated DNA was then size-selected on a 2% SizeSelect™ E-Gel (Invitrogen, Carlsbad, CA, USA) and amplified by PCR. Library quality was assessed by measuring nanomolar concentration and the fragment size in base pairs. Raw sequence data in Fastq format were assessed for quality (FastQC, http://www.bioinformatics.babraham.ac.uk/projects/fastqc/) and ribosomal RNA content. NovoAlign version 2.08 (Novocraft, http://novocraft.com) was used to align reads to the reference genome. Parameters were trained to maximize sensitivity while maintaining the highest specificity for this data set. Resulting alignments were combined to create clusters of reads, which represent non-redundant genomic regions in the reference genome sequence. Cluster boundaries are created by taking all samples into account during the cluster generation to define the left-most and right-most end co-ordinates of each cluster. Only uniquely mapping reads are taken into consideration. Clusters then undergo linear normalization by multiplying each sample's locus coverage by the total reads of the lowest read-count sample divided by the respective sample's total reads. The normalized expression data are the basis for the expression comparison.

2.3 Bioinformatic analysis

The 75 bp single-end sequencing data generated with Illumina NextSeq were mapped to *Mus musculus* mm10 reference genome using RNA-Seq aligner STAR (v2.4.2a).[35] The gene-based expression levels were quantified with feature Counts (subread v.1.5.0)[36] applying parameters '-s 2 –Q 10'. Read counts were normalized to the total number of sequencing reads falling into annotated gene regions in each sample, and further scaled based on a trimmed mean of log-transformed counts per million (CPM) value to correct for the variability of RNA composition in each sample.[37,38] The genes with expression greater than three per million mappable reads (CPM > 3) in at least three samples were kept for gene differential expression analysis with the R/Bioconductor package edgeR.[37] Two samples, one from the $Nkx2.5^{+/+}$; $Hand1^{f/f}$ group, and one from the $Hand1^{f/f}$ group, were removed from the differential gene expression analysis based on multidimentional scaling plot and *Hand1* gene expression level. Benjamini and Hochberg's algorithm was used to control the false discovery rate (FDR). Genes with a FDR <5% were considered differentially expressed. The differentially expressed genes were imported into Ingenuity Pathway Analysis (IPA, QIAGEN) for upstream regulator and disease and function analyses. Data are deposited at GEO and will be available 1 June 2019 at the following URL: https://www.ncbi.nlm.nih.gov/geo/query/acc.cgi?acc=GSE128571 (accession number GSE128571).

2.4 QRTPCR

QRTPCR was performed on a QuantStudio 3 (Applied Biosystems, Foster City, CA, USA) quantitative thermocycler using TaqMan primers (Life Technologies, Whitefield, Bangalore, Karnataka, India) recognizing the following transcripts: *Hand1, Hand2, Cited1, Nppa, Mybcp1, Hcn4, Gja5, Cxcl12, Tnni2, Itpr2, Crebbp, Adcy1, Phkg1, Ppp1r3a, Cacna1d, Plcb2,* and *Mapkapk3*. *Gapdh* is used in normalization. Error bars denote the maximum and minimum relative level of gene expression in the test samples calculated using the confidence level set in the QuantStudio 3&5 software analysis settings. *P* values ≤0.05 generated by the QuantStudio 3 software which calculates Benjamini–Hochberg FDR were regarded as

significant and marked in all graphs as a single asterisk (*) $n \geq 6$ in all experiments for all genotypes assayed.

2.5 Histology and morphometric analysis

Embryos (E9.5–E18.5) and adults were fixed in 4% paraformaldehyde, dehydrated, embedded, sectioned, and haematoxylin and eosin (H&E) stained as described.[22,31] A minimum of six viable embryos per genotype was used for all analyses. All data were collected on a Leica DM5000 B compound florescent microscope. For scoring the incidence of VSDs adult sections ($N = 20$ for *Nkx2.5*^{Cre} and $N = 12$ for *αMHC-Cre* generated *H1CKOs*) was calculated to be 0.7 and 0.5, respectively and show significant *P* values of 0.02 and 0.01, respectively using the Fisher's exact Test.

The Morphometric data were analysed following the established protocol as described.[39] To measure the wall and trabeculae thickness, four comparable levels of chamber cross-sections between the KO and control groups. Twelve to 20 spots along with the LV wall and RV wall were measured for the wall thickness for each section, and 20 to 42 measurements for trabecular thickness for each section. A Shapiro–Wilk test was applied to each set of measurements to test for normal distribution. For data sets fitting normal distribution, significance was calculated using unpaired *t*-test. The diameter of trabecular myocardium data set failed the normal distribution test and significance was determined by Mann–Whitney *U* test. All the measurements had same variances (*F* test, $P > 0.05$). $N = 12$ per genotype. Error bars represent standard deviation.

2.6 Immunofluorescence staining and confocal microscopy imaging for morphometric analysis

All images, confocal images, were obtained from single-laser layer scanning (unstacked, magnifications: 400X). CD31-positive (green) cells represent endocardium, while MF20 (red) cells are myocardium. Cardiac trabeculation and compaction were measured and calculated as previously described.[39] Staining and analysis procedures were as previously described.[39] Slides were dried for 30 min at room temperature (RT) and fixed for 10 min in cold acetone and washed 3 times in phosphate buffered saline (PBS) before being treated with blocking solution (M.O.M Kit, Vector Laboratories, Inc., Burlingame, CA, USA) for 1 h. Primary antibodies were added to a final concentration of 2 μg/mL for MF20 (MF20, DSHB, Iowa City, IA, USA) and 5 μg/mL for CD31 (AF3628, R&D Systems, Minneapolis, MN, USA) and incubated at 4°C overnight. About 1 μg/mL secondary antibodies (A21202 AND A11058, ThermoFisher Scientific, Waltham, MA, USA) were used and incubated for 1 h at RT followed by DAPI staining and mounting (P36931, ThermoFisher Scientific). PBS washes twice between each step. Samples were analysed using a Leica TCS SP8 confocal microscope and Leica Application Suite X. All images were from single-laser layer scanning (unstacked, magnifications: 400X). CD31-positive cells represent endocardium, while MF20 cells represent myocardium.

2.7 Echocardiography, electrocardiogram (ECG), and epicardial optical voltage mapping of Langendorff-perfused hearts

Adult mice (both sexes) of the indicated age were mice ($N = 12$ for 4-, 8-, and 12-week studies; $N = 6$ for $P \geq 210$ animals) are anaesthetized with isoflurane (2%) and oxygen (98%) mixture and assayed for cardiac function on either a Vevo 770 or Vevo 2100 ultrasound machine as described.[30,40,41] Functional analysis was performed by a single user (WZ) for consistency. One-way analysis of variance (ANOVA) determined statistical significance with a $P \leq 0.05$ confidence.

2.8 ECG

Surface ECGs were performed on mice that were lightly anaesthetized with 2% isoflurane mixed with O_2. Mice were mounted on a heated stage and temperature and heart beat were monitored during recording. ECGs were recorded for 1 min at a sampling rate of 2000 Hz using the PowerLab26T (ADInstruments, Colorado Springs, CO, USA). QT_c was calculated using LabChart software package (ADInstruments, Colorado Springs, CO, USA) using the equation $QT_c = QT/(RR/100)^{1/2}$, where QT is the measured Q-T interval and RR is the measured R-R interval.[42] ECG intervals were measured by averaging 100 beats using LabChart software package. Statistical analysis was performed first by employing a Shapiro–Wilk test to test for normal distribution and when normal distribution was established, we next employed one-way ANOVA with *post hoc* Tukey HSD test to determine significance (*$P \leq 0.05$, **$P \leq 0.01$).

2.9 Optical voltage mapping

High-resolution optical mapping experiments were performed on 6-month-old *Hand1*$^{f/f}$ controls, *Nkx2.5*$^{Cre/+}$;*Hand1*$^{+/+}$ and *Nkx2.5*$^{Cre/+}$;*Hand1*$^{f/f}$ CKOs using littermates as described previously.[43] Hearts were isolated and retrogradely perfused in Langendorff-mode with temperature-controlled (37°C) Krebs–Henseleit solution (pH 7.4 when gassed with a mixture of 95% O_2 and 5% CO_2) at an aortic pressure of 70 cmH_2O. A volume-conducted ECG was monitored continuously throughout the experiment. After 10 min of stabilization, the hearts were stained with the voltage-sensitive dye Di-4-ANEPPS (2 μL of a 2-mmol/L stock solution). The heart was then washed with dye-free solution for 5 min followed by the addition of (±)-blebbistatin to uncouple contraction from excitation (10 μmol/L; Tocris Bioscience, Minneapolis, MN, USA). The stained hearts were illuminated with a laser at a 532 nm wavelength and the fluorescence was collected by a MiCAMUltima-L CMOS camera (SciMedia, Costa Mesa, CA, USA) through a 715-nm long-pass filter. The fluorescence was recorded at a 1 ms/frame rate in a 100 × 100-pixel grid with a spatial resolution of 0.35 × 0.35 mm^2 per pixel. Optical signals were processed with both spatial (3 × 3 pixels Gaussian filter) and temporal (three frames moving average) filtering. Hearts were paced at the right atrium at a cycle length of 120 ms. Three 1-s recordings were captured sequentially, while the right atrium was paced at cycle lengths of 120, 150, and 200 ms. This protocol was repeated once. Finally, three 1-s recordings were acquired, while the hearts were paced from the apex at cycle lengths of 120, 150, and 200 ms. Activation time was measured as described previously.[43] The prevalence of RBB was determined significant by $P = 0.015$ using a χ^2 test.

3. Results

3.1 Transcriptome analysis of E11.5 H1CKO ventricles reveals that several gene regulatory networks indicative of cardiac dysfunction are altered

To look at the role of HAND1 in cardiomyocytes during development, we intercrossed *Hand1* conditional knockout mice[23] with either *Nxk2.5*^{Cre}[33] or *αMhc-Cre*[34] driver mouse lines. Assessment of recombination was assayed by both wholemount *in situ* hybridization (ISH) as this *Nxk2.5*^{Cre}[23] has not been utilized previously for *Hand1* ablation

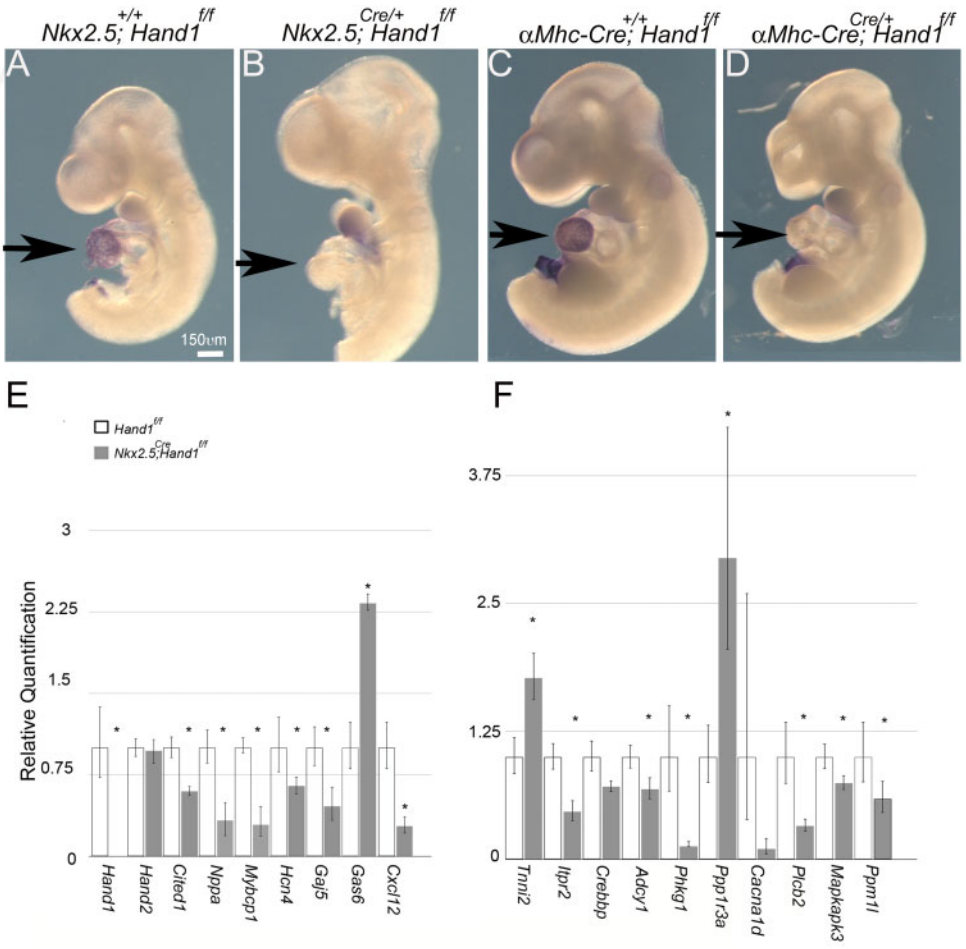

Figure 1 Cardiomyocyte-specific deletion of *Hand1*$^{f/f}$ and validation of select genes from transcriptome analysis of *Nkx2.5*$^{Cre/+}$;*Hand1*$^{f/f}$ mutant hearts. (*A*) Wholemount *in situ* hybridization of control E10.5 embryo showing *Hand1* LV expression (arrows). (*B*) *Nkx2.5*^{Cre}; *Hand1*$^{f/f}$ E10.5 embryo shows a loss of visible *Hand1* LV expression. (*C*) A similar *Hand1*$^{f/f}$ control as shown in *A*. (*D*) *αMhc-Cre*; *Hand1*$^{f/f}$ embryo shows a loss of visible *Hand1* LV expression. (*E*) QRTPCR analysis was performed from E11.5 ventricle cDNA from *Hand1*$^{f/f}$ control and *Nkx2.5*$^{Cre/+}$;*Hand1*$^{f/f}$ mutant hearts. Candidate expression analysis of genes associated with HAND1 regulation or not associated with an IPA biofunction category. (*F*) Expression analysis of genes chosen for protein kinase A and cardiac hypotrophy biofunctions. Error bars represent the minimum and maximum relative level of gene expression. $N \geq 6$ (six mutants and six control hearts/primer set). Error bars denote the maximum and minimum relative level of gene expression in the test samples calculated using the confidence level set in the QuantStudio 3&5 software analysis settings. *P* values ≤0.05 generated by the QuantStudio 3 software which calculates Benjamini–Hochberg false discovery rate were regarded as significant and marked in all graphs as a single asterisk (*) $n \geq 6$ in all experiments for all genotypes assayed. Scale bars = 150 μm.

(*Figure 1*). Additionally, we do not employ the systemic *Hand1* knockout allele[21] in this study, thus requiring two Cre-mediated recombination events to achieve Hand1 null cardiomyocytes compared to the study of McFadden *et al.*[23] These variations in approach and the inevitable changes in genetic background over extended breeding, likely account for the differences in our data.[20,44] Results show that *Hand1* expression at E10.5 is specifically deleted within LV cardiomyocytes using either *Nxk2.5*^{Cre} (*Figure 1A* and *B*) or *αMhc-Cre* (*Figure 1C* and *D*; black arrows). *Hand1* expression within the pharyngeal arches and umbilical area show deletion is conditional.

To gain an unbiased assessment of the changes in embryonic gene expression (both direct and indirectly regulated by HAND1), we isolated mRNA from E11.5 RV and LV and performed RNA-Seq analysis comparing *Nkx2.5*$^{Cre/+}$;*Hand1*$^{+/+}$ controls with *Nkx2.5*$^{Cre/+}$;*Hand1*$^{f/f}$ CKOs. We chose E11.5 as it represents the peak of *Hand1* expression prior to its down-regulation.[20,44] IPA for disease and biofunction identified a number of pathways with a *Z* score of greater than |2| as summarized in *Table 1*.

Alterations were seen in several diseases and biofunction classes associated with adult cardiac failure including *Nfat in Cardiac hypertrophy*, *Cardiac hypertrophy*, *Cardiac β-adrenergic Signalling*, and *Renin-Angiotensinogen Signalling* as shown by changes in gene expression within E11.5 day ventricles between control and *Nkx2.5*$^{Cre/+}$;*Hand1*$^{f/f}$ CKOs hearts. Interestingly, EIF2 signalling, associated with protein translation (required for increased muscle mass), is the most significantly (*Z* score 5.048; *Table 1*) changed pathway. To validate the accuracy of RNA-Seq analysis, we performed QRTPCR on select candidate genes from these pathways. As expected, results show *Hand1* expression is decreased beyond detection in knockout samples vs. controls (*Figure 1E*). *Hand2* expression is unaffected and consistent with previous studies the Hand1

Table 1 Canonical pathways significantly altered in *Nkx2.5*$^{Cre/+}$;*Hand1*$^{f/f}$ E11.5 hearts

IPA class	−log(*P* value)	Ratio	|*Z*-score|
Role of NFAT in cardiac hypertrophy	1.31E+00	1.03E-01	2.000
Agrin interactions at neuromuscular junction	3.3E-01	7.58E-02	2.000
Dendritic cell maturation	3.3E-01	7.19E-02	2.111
Protein kinase A signalling	2E-00	1.01E-01	2.117
Paxillin signalling	1.83E-00	1.33E-01	2.121
Aldosterone signalling in epithelia cells	1.11E-00	1.01E-01	2.121
Melanocyte development and pigmentation signalling	9.6E-01	1.08E-01	2.121
FLT3 signalling in haematopoietic progenitor cells	8.92E-01	1.08E-01	2.121
Cardiac hypertrophy signalling	2.8E-00	1.25E-01	2.132
Basal cell carcinoma signalling	4.7E-01	18.57E-02	2.236
TGF-β signalling	2.82E00	7.06E-02	2.236
STAT3 PATHWAYS	2.53E-01	6.85E-02	2.236
CDK5 signalling	1.54E-00	1.25E-01	2.309
Glioblastoma multiform signalling	5.64E-01	8.33E-02	2.309
NF-κB signalling	3.59E-00	7.32E-02	2.309
α-adrenergic signalling	1.24E-00	1.19E-01	2.449
Dopamine receptor signalling	1.17E-00	1.2E-01	2.449
IL-1 signalling	1.1E-00	1.12E-01	2.449
Wnt/Ca+ pathway	7.49E-01	1.07E-01	2.449
Dopamine-DARPP32 feedback in cAMP signalling	3.02E-00	1.5E-01	2.524
Ephrin receptor signalling	9.21E-01	9.36E-02	2.53
Neuropathic pain signalling in dorsal horn neurons	8.92E-01	1.02E-01	2.53
Cardiac β-adrenergic signalling	3.03E-00	1.5E-01	2.673
Renin–angiotensin signalling	9.58E-01	1.03E-01	2.714
CREB signalling in neurons	2.99E00	1.37E-01	3.051
GNRH signalling	1.11E-00	1.06E-01	3.051
Synaptic long-term potentiation	1.89E-00	1.28E-01	3.207
EIF2 signalling	3E+01	3.73E-01	5.048

transcriptional targets *Cited1* and *Nppa* are down-regulated.[23,30] Other validated genes showing significant reduction in expression include: *Myosin binding protein C1* (*Mybpc1*), a gene associated with slow twitch muscle, that is, dramatically, down-regulated in engineered cardiac tissue upon p38MAPK inhibition,[45] that is, causative of cardiac oedema and bradycardia when knocked down in zebrafish,[46] as well as highly expressed in human hearts throughout the first trimester[47]; *Hcn4*, *Hyperpolarization Activated Cyclic Nucleotide Gated Potassium Channel 4*, the potassium/sodium channel associated with LV non-compaction and conduction system function[48]; CONNEXIN40 (*Gja5*) a tight junction protein also associated with conduction system development; and[49] *Growth arrest-specific 6* (*Gas6*), also associated with vascular formation[50] and robustly expressed in the heart[51] (*Figure 1E*). *Cxcl12* expression, a maturation factor required for coronary vessel development,[52,53] is also significantly down-regulated in our mutant ventricles by both RNA-Seq analysis and QRTPCR (*Figure 1E*) similar to what we have previously observed in Hand factor LV deletion mice.[30]

To further validate the transcriptome data and gain insight into the gene regulatory networks revealed in the IPA, we next focused on biofunctions that involved protein kinase A (PKA) signalling, a well-established mechanism for Hand factor functional regulation,[54] and pathways related to cardiac hypertrophy (*Figure 1F*). The contractile gene *Troponin I type 2* (*Tnni2*), associated with PKA biofunctions is significantly up-regulated in *Nkx2.5*$^{Cre/+}$;*Hand1*$^{f/f}$ mutant hearts. *Inositol 1, 4,5-trisphosphate receptor, type 2*, (*Itpr2*) a regulator of transportation activity across the sarcoplasmic reticulum membrane, is significantly down-regulated. *cAMP response element-binding protein binding protein* (*Crebbp*), is a transcriptional co-activator that is down-regulated close to significant levels ($P = 0.063$). *Adenylyl cyclase type 1 (Adcy1)* and *Phosphorylase b kinase gamma catalytic chain* (*Phkg1*) are both significantly down-regulated in *Nkx2.5*$^{Cre/+}$;*Hand1*$^{f/f}$ mutant hearts (*Figure 1F*).

Genes associated with β-adrenergic signalling and/or cardiac hypertrophy validated by QRTPCR include: *Protein phosphatase 1 regulatory subunit 3A* (*Ppp1r3a*) which is significantly elevated in expression in *Nkx2.5*$^{Cre/+}$;*Hand1*$^{f/f}$ mutants; *Calcium voltage-gated channel subunit alpha 1d* (*Cacna1d*) is down-regulated ($P = 0.063$), *phospholipase C beta2* (*Plcb2*) a gene also associated with PKA signalling, and *Map kinase-activated protein kinase 3* (*Mapkapk3*), a MAP kinase pathway driver are both significantly down-regulated in *Nkx2.5*$^{Cre/+}$;*Hand1*$^{f/f}$ mutant hearts. Protein phosphatase 1-like (*Ppm1l*) localizes to the endoplasmic reticulum (ER) modulating ER-stress[55] and thus influencing hypertrophy. *Ppm1l* is significantly down-regulated in *Nkx2.5*$^{Cre/+}$;*Hand1*$^{f/f}$ mutant hearts (*Figure 1F*). Together, this analysis shows that *Hand1* loss in cardiomyocytes alters cardiac embryonic gene regulatory networks commonly found dysregulated in adult cardiac hypertrophy and heart disease.

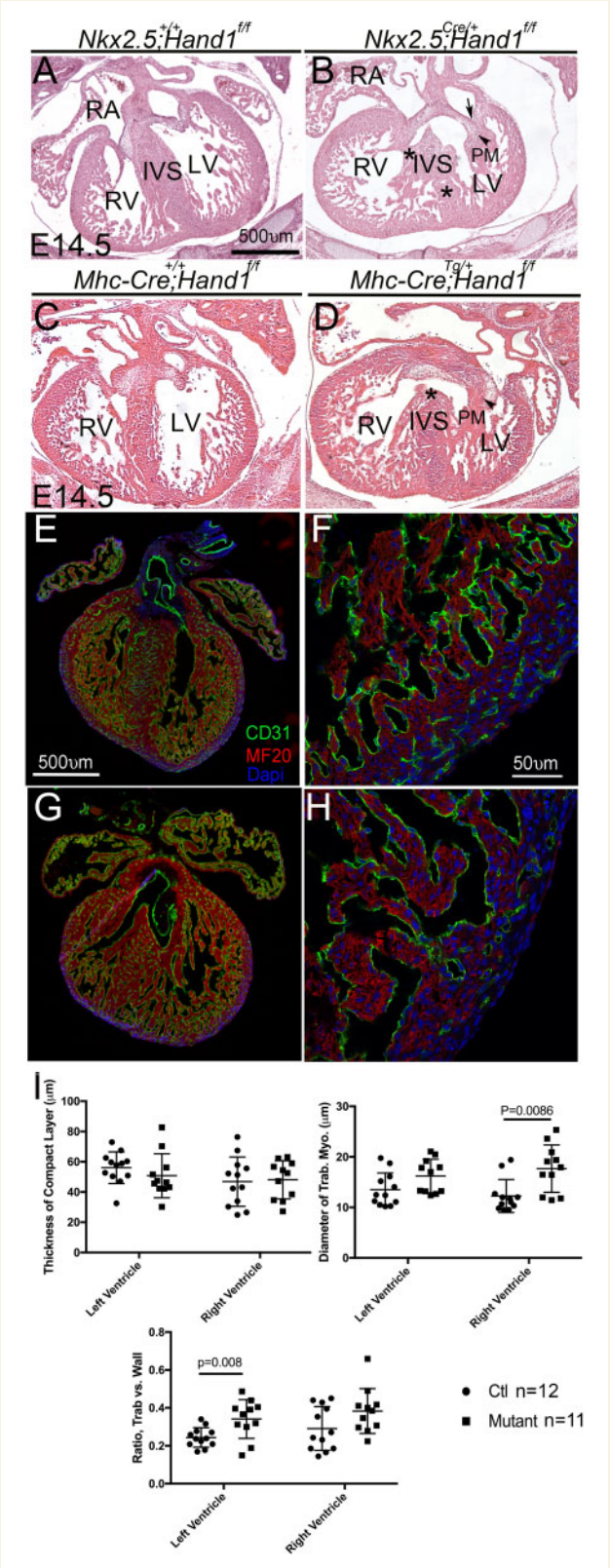

Figure 2 Histological assessment of cardiac morphology reveals morphological defects in E14.5 H1CKOs hearts. H&E stained control E14.5 *Hand1*$^{f/f}$ hearts (*A*, $n \geq 10$ and *C*, $n \geq 10$) compared to *Nkx2.5*^{Cre}; *Hand1*$^{f/f}$ (*B*, $n \geq 10$); and *αMhc-Cre*; *Hand1*$^{f/f}$ (*D*, $n \geq 10$) embryos. Control heart morphology shows distinct RV and LV and patent IVS. In *Nkx2.5*^{Cre}; *Hand1*$^{f/f}$ mutants, ventricular septal defects are visible (asterisk), mitral valves appear immature (arrow), PM in *B* directly attaches to the valve (arrowhead). *αMhc-Cre*; *Hand1*$^{f/f}$ mutants (*D*) display similar ventricular septal defects (asterisks) and a PM directly inserting into the mitral valve (arrowhead $n \geq 10$). Scale bars = 500 µm. Frequency of VSD occurrence was calculated to be 0.7 for *Nkx2.5*^{Cre} generated and 0.5 for *αMHC-Cre* generated *H1CKOs* and exhibit significance with *P* values of 0.02 and 0.01, respectively obtained using the Fisher's exact Test. (*E–H* all $n = 12$ for controls $n = 11$ for mutants) immunohistochemistry sections of *Control* (*E* and *F*) and *H1CKO* (*G* and *H*) showing expression of the endothelial-specific protein CD31 (green) the cardiomyocyte-specific antibody to αMHC (MF20, red) and nuclei are visualized by DAPI staining (Blue). (*I*, $n = 12$ for control; $n = 11$ mutants). Sections were used to calculate the thickness of the LV and RV compact walls, RV and LV trabecular diameter, and the ratio of trabecula to compact wall. A Shapiro–Wilk test was applied to each set of measurements to test for normal distribution. All data sets fitting normal distribution were tested for statistical significance was calculated using unpaired *t*-test $n = 12$ for control and $n = 11$ mutant hearts. Measure of diameter of trabecular myocardium failed the normal distribution test, and significance was determined by Mann–Whitney *U* test. Scale bars = 500 and 50µm where indicated. Error bars represent standard deviation.

3.2 Analysis of *H1CKO* embryos shows the presence of ventricular septal defects and an increased trabecular to compact zone ratio

We next isolated E14.5 embryos and looked at cardiac histology via H&E staining (*Figure 2*). Results show that consistent with previous findings,[23] *Nkx2.5*^{Cre} *H1CKOs* embryos exhibit membranous ventricular septal defects (VSDs, asterisks; frequency 0.7; $N = 20$, $P = 0.02$ Fisher's exact test) and present with large immature mitral valves (MVs; *Figure 2A* and *B* arrow). *Mhc-Cre-H1CKOs* present with similar phenotypes (*Figure 2C* and *D*; frequency 0.5; $N = 12$, $P = 0.014$ Fisher's exact test). We next performed morphometric analysis to determine both trabecular and compact wall thicknesses from immunoreacted sections (*Figure 2E–I*). Antibodies for CD31 (green) and αMHC (red) were reacted on sections from E14.5 control *Hand1*$^{f/f}$ to *Nkx2.5*^{Cre}*-H1CKOs* hearts. Results show that compact wall thickness is indistinguishable within the RV and LV walls of *Nkx2.5*^{Cre}*-H1CKOs* hearts (*Figure 2I*). In contrast, diameter of trabecular myocardium between *Hand1*$^{f/f}$ and *Nkx2.5*^{Cre}*-H1CKOs* hearts was found significantly thicker in the RV ($P = 0.004$) and the ratio of trabecular tissue to compact wall myocardium is significantly increased within the LV of *Nkx2.5*^{Cre}*-H1CKOs* heart ($P = 0.008$; *Figure 2I*). Previous cell lineage analysis using *Hand1*^{eGFPCre} shows that within the heart, *Hand1*-lineage is restricted to the compact zone, trabecular, and small domain within the IVS myocardium of the LV and within myocardial cuff of the RV with no detectable expression observed within the endocardium.[56,57] Although the *Hand1*-lineage directly contributes to the epicardium, *Hand1* is not expressed within the proepicardial organ or epicardium.[56,57] These observations suggest that the observed CHDs observed in *H1CKOs* are cell autonomous to the myocardium and that cardiomyocyte deletion of *Hand1* results in an increase of LV trabecular tissue and that VSD and valve phenotypes are consistent with similar published embryonic analysis.[23]

3.3 Functional analysis of *H1CKO* hearts reveals defects in cardiac conduction

We next intercrossed *Cre*$^{+/-}$; *Hand1*$^{fl+}$ males with *Hand1*$^{f/f}$ females and genotyped P10 offspring. Results from over 40 pups show surviving Cre$^{+/-}$; *Hand1*$^{f/f}$ *H1CKOs* at expected Mendelian frequencies using either *Cre* driver (Supplementary material online, *Table S1*). Neonatal *H1CKOs* survived to adulthood and were fertile. Although McFadden *et al.*[23] report only less than ~5% viability using *αMHC*-Cre (and no survival with *Nkx2.5-Cre*), their study utilized a *Hand1*$^{LacZ/fx}$ genetic combination and a transgenic *Nkx2.5-Cre* driver vs. in our study, we utilized only *Hand1*$^{f/f}$ genetic combination and the knockin *Nkx2.5*^{Cre} driver. In our observations, mice survive beyond 12 months of age and do not appear to suffer from premature early death.

Given that the *H1CKO* transcriptome data showed alterations in the expression of several cardiac conduction system genes and we validated three of the identified genes by QRTPCR (*Figure 1E*), we looked at cardiac conduction in adult mice using surface ECG analysis (*Figure 3A–C*). Results show that when compared with *Nkx2.5*$^{Cre/+}$ and *Hand1*$^{f/f}$ controls *Nkx2.5*$^{Cre/+}$;*Hand1*$^{f/f}$ mutants exhibit an indistinguishable PR and QT interval; however, a longer QRS interval is observed in *Nkx2.5*$^{Cre/+}$;*Hand1*$^{f/f}$ mutants in lead I QRSII ($P \leq 0.05$), lead II QRSII, ($P \leq 0.05$), and lead III QRSI ($P \leq 0.01$) measures (*Figure 3A–C*).

We next employed optical voltage mapping of isolated perfused hearts to more accurately interrogate the altered QRS durations observed in the *Nkx2.5*$^{Cre/+}$;*Hand1*$^{f/f}$ mutants (*Figure 3D–I*). While pacing the right atria, the majority of control *Hand1*$^{f/f}$ hearts ($n = 4$, 6 total) exhibited two breakthrough sites on the anterior surface (near the apex of the RV and LV; *Table 2*). The breakthroughs occurred simultaneously (within the temporal resolution of our imaging system). While pacing the ventricle at the apex, activation propagated towards the base with similar speed in the RV and LV. The Supplementary material online, *Movie S7* shows a representative example of the epicardial activation patterns in a *Hand1*$^{f/f}$ heart. One control *Hand1*$^{f/f}$ heart was observed to exhibit a single LV epicardial breakthrough site with no observable RV breakthrough during atrial pacing (*Figure 3D*; Supplementary material online, *Movie S1*), while another control *Hand1*$^{f/f}$ heart exhibited two LV epicardial breakthrough sites along with a singular RV breakthrough site. RV breakthrough was delayed (*Figure 3E*; Supplementary material online, *Movie S2*). Both of these two *Hand1*$^{f/f}$ controls exhibited epicardial activation patterns that were indistinguishable from those seen in the other four *Hand1*$^{f/f}$ hearts during pacing at the ventricular apex (*Table 2*). Two out of four *Nkx2.5*$^{Cre/+}$ control hearts exhibited simultaneous RV and LV epicardial breakthroughs while being paced from the right atria and normal apex-to-base propagation patterns when paced from the ventricular apex (*Table 2*). One *Nkx2.5*$^{Cre/+}$ control heart exhibited single LV and RV breakthrough sites and another *Nkx2.5*$^{Cre/+}$ control mouse exhibited two LV and two RV epicardial breakthrough sites when paced from the atria (*Figure 3F* and *G*; Supplementary material online, *Movies S3* and *S4*). Again, both of these *Nkx2.5*$^{Cre/+}$ control hearts showed the expected propagation of epicardial activation when paced from the ventricular apex (*Table 2*). These results show that although the majority of *Hand1*$^{f/f}$ and *Nkx2.5*$^{Cre/+}$ control mice display a normal epicardial activation pattern when paced from the right atria, a small fraction of the control hearts do display conduction phenotypes that are not detectable by surface ECG analysis and this needs to be considered when evaluating mutant phenotype.

In contrast to the control groups, all six *Nkx2.5*$^{Cre/+}$;*Hand1*$^{f/f}$ mutants assayed display abnormal epicardial activation patterns during atrial pacing. All *Nkx2.5*$^{Cre/+}$;*Hand1*$^{f/f}$ mutants exhibit either one or two LV epicardial breakthrough sites with no observable RV breakthrough (*Figure 3H* and *I*; Supplementary material online, *Movies S5* and *S6*), while activation was unimpaired during pacing at the ventricular apex when compared with the epicardial activation pattern in a *Hand1*$^{f/f}$ heart (*Table 2*). These data show that in addition to the observed structural defects *Nkx2.5*$^{Cre/+}$;*Hand1*$^{f/f}$ mutants display abnormal epicardial activation patterns consistent with the presence of a right bundle branch block caused by a combination of defective morphology and altered regulation of conduction system gene expression.

3.4 *Nkx2.5*^{Cre}; *Hand1*$^{f/f}$ mice exhibit persistent VSDs, abnormal growth of LV papillary muscles, and cardiomegaly

A number of adults (6–8 months of age) *H1CKO* mice exhibited signs of lethargy as compared to their *Hand1*$^{f/f}$ littermates; therefore, we examined the hearts in these *H1CKO* mice (*Figure 4*). Results show a pronounced cardiomegaly ($n \geq 100$) in *Nkx2.5*$^{Cre/+}$;*Hand1*$^{f/f}$ mice when compared with *Hand1*$^{f/f}$ littermates. Both RV and LV are visibly hypertrophic and the left atrium (LA) is also enlarged (*Figure 4A* and *B*). *Nkx2.5*^{Cre} *H1CKO* hearts lack a clearly identifiable apex (*Figure 4B*). Histology shows both membranous (large arrowhead) and muscular (small arrowheads) VSDs accompanied by hypertrophic RV, LV, and dilated LA myocardium (*Figure 4C* and *D*). Interestingly, the extent of the hyper-muscularized RV free wall suggests that the VSD was large enough to be haemodynamically significant, resulting in increased RV volume and/or pressure overload. Frequently, the LV papillary muscles (PMs) of the *Nkx2.5*^{Cre} *H1CKOs* appear to directly insert into the MV, a phenotype that is similar to a human condition called Mitral Arcade[58,59] (*Figure 4D* boxed and *D'* $n \geq 10$). Additionally, *Nkx2.5*^{Cre} *H1CKO* mice show pulmonary oedema (*Figure 4E* and *F*). These data suggest that *Nkx2.5*^{Cre} *H1CKO* adults develop lung congestion ($n \geq 10$ observed) and cardiomyopathy typically seen in CHD with left to right shunts from intracardiac defects.

We next looked at replacement fibrosis in *Nkx2.5*^{Cre}-generated *H1CKO* adults (≥p60). Sirius red staining of a typical *Nkx2.5*^{Cre} *H1CKO* shows significant levels of ventricular collagen deposition (*Figure 4G*). In addition, muscular VSDs (*Figure 4I* magnification of *4G*; black arrows), overtly hyper-muscularized RV free wall, and LV PM making direct contract with the MV (*Figure 4H* magnification of *4G* double asterisk) are apparent in this animal. The insertion of the PMs into the MV of *Nkx2.5*^{Cre} *H1CKOs* can also be visualized via ultrasound imaging (*Figure 4J* yellow arrowhead $n \geq 10$ by histological examination).

In the initial analysis of *Nkx2.5* loss-of-function mice, *Hand1* was reported as a regulated gene.[60] To confirm *Nkx2.5*^{Cre} *H1CKOs* phenotypes are not significantly influenced by *Nkx2.5* haploinsufficiency, we next examined *αMhc-Cre H1CKOs* (*Figure 5*). At P2, histological analyses reveal morphological abnormalities consistent within the LV that includes ectopic muscle within the lumen of the LV and a PM originating from the cardiac apex (*Figure 5B* asterisk). At P60, significant replacement fibrosis within the IVS is readily apparent in *αMhc-Cre(+)*; *Hand1*$^{f/f}$ hearts and the PM connections to the MV (*Figure 5C* arrowhead) appear to be similar to what we observe with the Nkx2.5^{Cre} *H1CKOs*.

Echocardiographic images of *Nkx2.5*^{Cre} *H1CKO* mice show visible membranous and muscular VSDs (*Figure 6A–C*). Colour and pulse wave Doppler measurements of an *Nkx2.5*^{Cre} *H1CKO* reveal a membranous VSD with an -1800 mm/s velocity (*Figure 6D*) as is shown in a colour Doppler movie of the VSD (*Nkx2.5*^{Cre} *H1CKO* Supplementary material online, *Movie S8*). Together, these data show that cardiomyocyte loss of

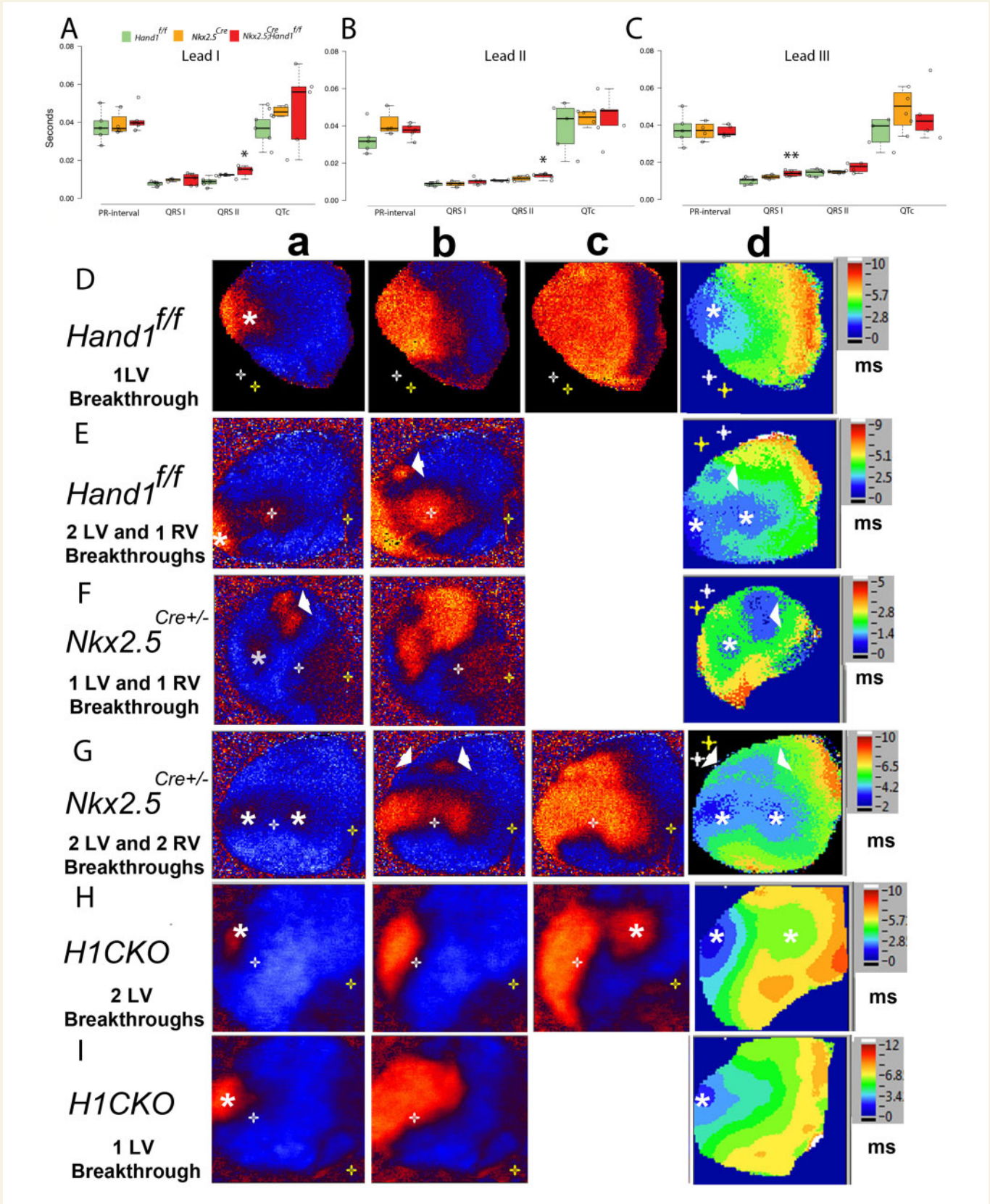

Figure 3 Functional analysis of *Nkx2.5*^{Cre}; *Hand1*$^{f/f}$ mice show altered ventricular conduction. (*A–C*) Surface ECG analysis of leads I, II, and III from anaesthetized mice. QT_c indicates corrected QT interval. A prolonged QRS duration is observed in Nkx2.5^{Cre}; *Hand1*$^{f/f}$ mice ($n = 6$) in all leads (either QRSI or QRSII) when compared with controls (*Hand1*$^{f/f}$ $n = 6$; *Nkx2.5*$^{Cre+/-}$ $n = 5$). A Shapiro–Wilk test was first applied to each set of measurements to test for normal distribution. Data were found to normal distribution and significance was determined using one-way ANOVA with *post hoc* Tukey HSD test. $^{*}P \leq 0.05$, $^{**}P \leq 0.01$. In the box-scatter plots centre lines indicate medians; box limits indicate the 25th and 75th percentiles; whiskers indicate the 1.5X the

Table 2 Summary of ventricular breakthrough sites observed in *H1CKOs*

Genotype	Number of ventricular breakthrough sites during right atrial pacing	Mean interval between earliest LV and earliest RV breakthrough (ms)
Hand1$^{f/f}$	1 LV, 1 RV (4/6 hearts)	0
Hand1$^{f/f}$	1 LV (1/6 hearts)	NA
Hand1$^{f/f}$	2 LV, 1 RV (1/6 hearts)	3
Nkx2.5$^{Cre+/-}$	1 LV, 1 RV (3/4 hearts)	0
Nkx2.5$^{Cre+/-}$	2 LV, 2 RV (1/4 hearts)	0
Nkx2.5$^{Cre+/-}$; *Hand1*$^{f/f}$	1 LV (3/6 hearts)	NA
Nkx2.5$^{Cre+/-}$; *Hand1*$^{f/f}$	2 LV (3/6 hearts)	NA

Negative value for the mean interval indicates that the activation was earliest in the LV. Optical voltage maps were obtained during right atrial pacing at a cycle length of 120 ms or 150 ms.
LV, left ventricular; RV, right ventricular.

Hand1 results in survivable VSDs and PM defects that alter the connection with the MV resembling Mitral Arcade.[58]

3.5 Functional analysis of *H1CKO* hearts reveals diastolic dysfunction that progresses to heart failure

In order to determine the aetiology of the heart failure observed in *H1CKO* mice, we undertook a functional time course between 4 and 12 weeks of age with 12 mice per genotype analysed (*Figure 7*). Control *Nkx2.5*$^{Cre/+}$;*Hand1*$^{+/+}$ and *Nkx2.5*$^{Cre/+}$;*Hand1*$^{f/f}$ animals were assayed for fractional shortening (FS) and ejection fraction (EF; *Figure 7B*). Over this time course no significant differences in systolic function are observed between control and *H1CKO* mice. We next looked at aortic (Ao) and pulmonary artery (PA) peak velocity (*Figure 7B*). Results show PA peak velocity was not significantly changed; however, Ao peak velocity is significantly higher in the *H1CKO* mice at 4 and 12 weeks. We next looked at diastolic function using tissue Doppler (*Figure 7C*). Results from this cohort of mice show that the MV A-wave velocity at 4 weeks (MV A; *Figure 7C*) and MV deceleration (MV Decel; *Figure 7C*) at 12 weeks is significantly altered in *Nkx2.5*$^{Cre/+}$;*Hand1*$^{f/f}$ when compared with controls. Calculation of the MV E/e' ratio reveals that this measure of increased atrial filling pressure is also significantly higher in *Nkx2.5*$^{Cre/+}$;*Hand1*$^{f/f}$ mice (*Figure 7C*) suggesting that *H1CKO* mice are presenting with HFpEF. Interrogation of older (≥P180) *Nkx2.5*$^{Cre/+}$;*Hand1*$^{f/f}$ mice reveals EA reversal (*Figure 6E*) and compromised systolic function reflected with EFs below 40% and FS of <20% (*Figure 6F*). Collectively, these data support that embryonic loss of *Hand1* alters key gene regulatory networks that impact heart morphology such that embryonic viability is not compromised but sustained cardiac function is pathologically impacted.

4. Discussion

We have discovered that deletion of the bHLH transcription factor HAND1 results in viable fertile mice with cardiac conduction defects and exhibit VSDs as well as PM abnormalities, which resemble the CHD Mitral Arcade. *H1CKOs* presented with right bundle branch block and a prolonged QRS interval, which are both arrhythmogenic conditions predictive of cardiac sudden death.[9–12] In humans, Mitral Arcade presents with large PMs and absent or reduced chordae tendineae such that the PMs directly insert into the MV. This morphology results in poor MV function and stenosis leading to heart failure.[61,62] Although Mitral Arcade is rare, enlarged LA has been observed in older patients.[63,64] Given that *H1CKOs* exhibit similar phenotypes and present first with diastolic dysfunction, followed by diminished systolic function, myocardial loss of HAND1 appears to phenocopy this congenital disease. *Hand1* is first detected during cardiac development at E8.0.[57] *Nkx2.5*^{Cre} and *αMHC-Cre* express Cre at E7.5 and E9.5, respectively.[33,34] The use of these two drivers does not give rise to significant variations in the mutant phenotype, suggesting that potential genetic interactions between *Nkx2.5 and Hand1* in the genesis of phenotype are minimal.

The original cardiomyocyte-specific knockout using the *Hand1* conditional allele reports identical embryonic phenotypes to what is presented here; however, in our study *H1CKO* mice survive more robustly.[23] We feel that the difference can be accounted for by the different Nkx2.5 Cre drivers employed, as well as the inclusion of the *Hand1*^{LacZ} allele[21] in the earlier study making *Hand1* deletion more efficient. Indeed, when we utilized the *Hand1*^{LacZ} in crosses our frequency of *H1CKOs* encountered dropped to 11% (data not shown). We also suspect that 14 years of allele maintenance resulted in background drifting that may significantly contribute to the more robust survival observed in these data.

At E14.5 VSDs are clearly observable in *Nkx2.5*$^{Cre/+}$;*Hand1*$^{f/f}$ hearts in line with previous findings on similar *H1CKO* analysis validating the

Figure 3 Continued
interquartile range from the box limits; dots show number of animals $n \geq 5$. (*D–I*) Epicardial activation patterns in adult *Hand1*$^{f/f}$ ($n = 6$ each; *D* and *E*), *Nkx2.5*$^{Cre+/-}$ ($n = 5$ each; *F* and *G*) and Nkx2.5^{Cre}; *Hand1*$^{f/f}$ hearts ($n = 6$ each; *H* and *I*) during atrial pacing. Shown are representative sequential optical maps (columns a–c) and the colour-coded activation maps (column d) for each genotype. LV and RV breakthroughs are demarked by asterisks and arrowheads, respectively. Optical maps were obtained during right atrial pacing at a cycle length of 120 ms or 150 ms. (*D* and *E*) One *Hand1*$^{f/f}$ heart showed a single breakthrough site on the anterior LV surface (*D*) consistent with the presence of a right bundle branch block, while another *Hand1*$^{f/f}$ heart showed two and one breakthrough sites on the left and right ventricular surface (*E*), respectively. (*F* and *G*) In *Nkx2.5*$^{Cre+/-}$ hearts, epicardial breakthrough occurred first on the right anterior surface (*F*) or manifested as double breakthrough sites on both the left and right ventricular anterior surfaces (*G*). (*H* and *I*) Three out of six Nkx2.5^{Cre}; *Hand1*$^{f/f}$ (*H1CKO*) hearts showed two left ventricular breakthrough sites (*H*). The activation of the mid-anterior LV was grossly delayed (~3 ms). The remaining three Nkx2.5^{Cre}; *Hand1*$^{f/f}$ hearts exhibited single left ventricular breakthrough sites (*I*) indicative of right bundle branch block. Isochrone lines (*I* column d) demonstrate that LV global activation propagates from the LV to the RV. The prevalence of RBB was significantly higher in Nkx2.5^{Cre}; Hand1$^{f/f}$ hearts compared with both Nkx2.5^{Cre} and Hand1$^{f/f}$ hearts ($P = 0.002$ by χ^2 test followed by Fisher's Exact tests for pairwise comparisons). Cross hairs present in some of the images are cursors and do not highlight any data. (*D–I*) *Hand1*$^{f/f}$ ($n = 6$; *D* and *E*), *Nkx2.5*$^{Cre+/-}$ ($n = 5$; *F* and *G*) and Nkx2.5^{Cre}; *Hand1*$^{f/f}$ hearts ($n = 6$; *H* and *I*).

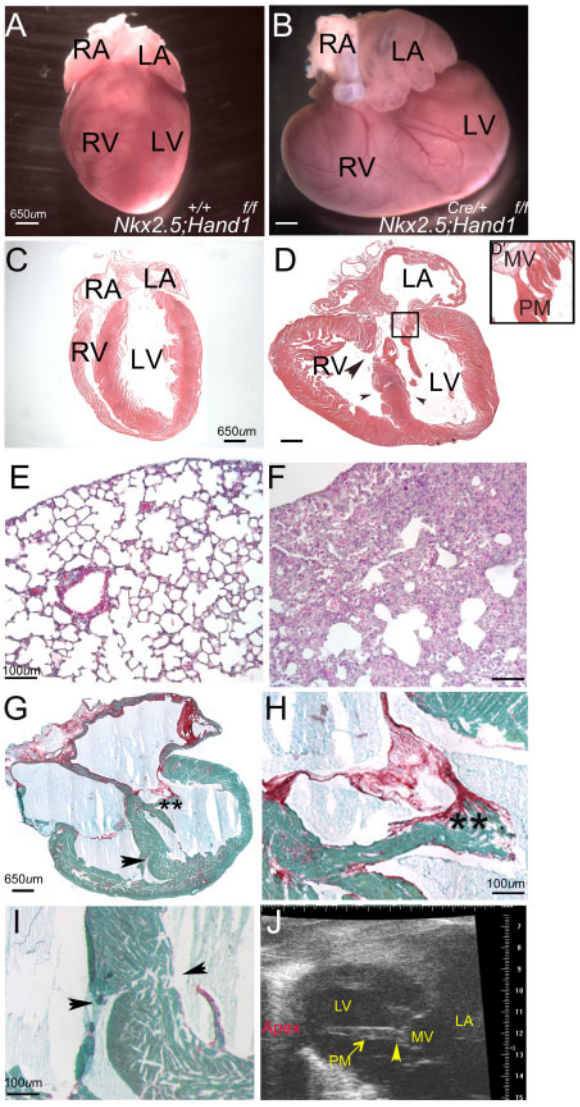

Figure 4 Adult (P60) *Nkx2.5*^{Cre}; *Hand1*$^{f/f}$ mice exhibit cardiomegaly and mitral arcade. (*A*) Control *Hand1*$^{f/f}$ heart with unremarkable RA and LA and RV and LV. (*B*) *Nkx2.5*^{Cre}; *Hand1*$^{f/f}$ heart is large and highly muscularized with a dilated LA, as well as RV and LV showing hypertrophic growth. (*C*) H&E section analysis of a control *Hand1*$^{f/f}$ heart shows normal chamber size and compaction. (*D*) *Nkx2.5*^{Cre}; *Hand1*$^{f/f}$ heart displays thickened ventricular walls and both membranous (large arrowhead) and muscular (small arrowheads) VSDs. Boxed area in *D* is magnified in *D*' showing PMs directly inserted into the mitral valve. (*E*) Control *Hand1*$^{f/f}$ lung showing normal morphology. (*D*) *Nkx2.5*^{Cre}; *Hand1*$^{f/f}$ lung presents with marked pulmonary oedema. (*G*) A second *Nkx2.5*^{Cre}; *Hand1*$^{f/f}$ example stained with Sirus red/fast green. VSD marked by arrowhead. Asterisks in *G* (magnified in *H*) show PM insertion into the mitral valve. (*I*) Magnified view of VSD shown in (*G*). (*J*) Echocardiography still image of a *Nkx2.5*^{Cre}; *Hand1*$^{f/f}$ mutant show a large PM directly inserted into the MV (yellow arrowhead). Scale bars *A–D* and *G*, 650 μm; Scales bars *E*, *F*, *H*, and *I*, 100 μm. $N \geq 10$.

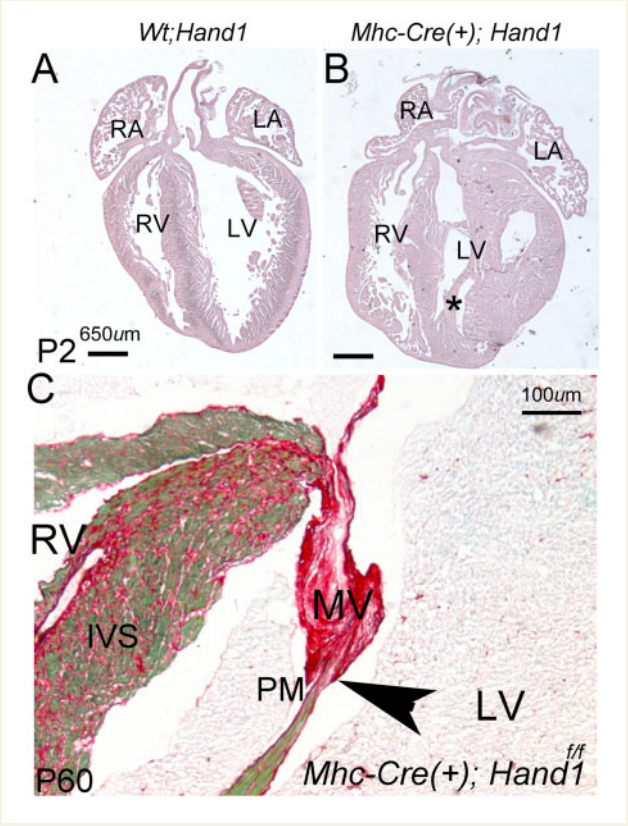

Figure 5 αMhc-Cre; *Hand1*$^{f/f}$ mice exhibit cardiomegaly and mitral arcade. (*A*) P2 H&E histology shows normal heart morphology. (*B*) αMhc-Cre; *Hand1*$^{f/f}$ mutant hearts display muscle overgrowth in the LV lumen and enlarged LA. (*C*) P60 Sirus red fast green stained αMhc-Cre; *Hand1*$^{f/f}$ mutant heart showing PM insertion into the MV and high levels of fibrosis in the IVS. Scale bars *A* and *B* 650 μm; Scales bars *C* 100 μm. $N \geq 10$.

congenital origins of the morphological defects (*Figure 2*).[23] We show here through morphometric analysis that E14.5 *Nkx2.5*$^{Cre/+}$;*Hand1*$^{f/f}$ hearts exhibit a significant increase in diameter of RV trabecular myocardium ($P = 0.004$; $n = 12$) as well as an increase in the ratio of trabecular to compact LV myocardium ($P = 0.008$; $n = 12$). The effect on RV trabecular diameter is likely non-cell autonomous given *Hand1* RV expression is restricted to the myocardial cuff.[20–22] However, LV morphological changes are likely to be cell autonomous effects. Indeed, both PM anomalies and survivable VSDs (*Figure 4A–C*) with high-velocity flow (*Figure 6D*) are present in adult *H1CKO* and these primary embryonic defects, over time, manifest adaptive non-cell autonomous phenotypes as a result of compromised cardiac function. These observations are completely novel and *H1CKOs* are a viable mouse model of congenital defects that lead heart failure in adults.

H1CKOs display enlarged LA, and hypertrophic RV and LV myocardium. Functional data from younger mice show that initially systolic function is not compromised (*Figure 7*). Aortic peak velocity is increased. Atrial Doppler patterns across the MV indicate of a stiff myocardium and poor MV function, which would be expected for a phenocopy of Mitral Arcade.[61] *H1CKO* mice exhibit E/A reversal (*Figure 6E*), enlarged LA, and in older mice ($P \geq 120$) systolic function becomes compromised (*Figure 6F*) fitting a diagnosis of HFpEF.[65] The LA-LV pressure imbalance in such cases of mitral stenosis in humans is alleviated partially by valvuloplasty.[66] Indeed, the pulmonary oedema observed (*Figure 4E* and *F*) is likely caused from pulmonary over-circulation from the resultant VSD.

In conjunction with these morphological and functional observations, we also observe using surface ECG and optical mapping that ventricular

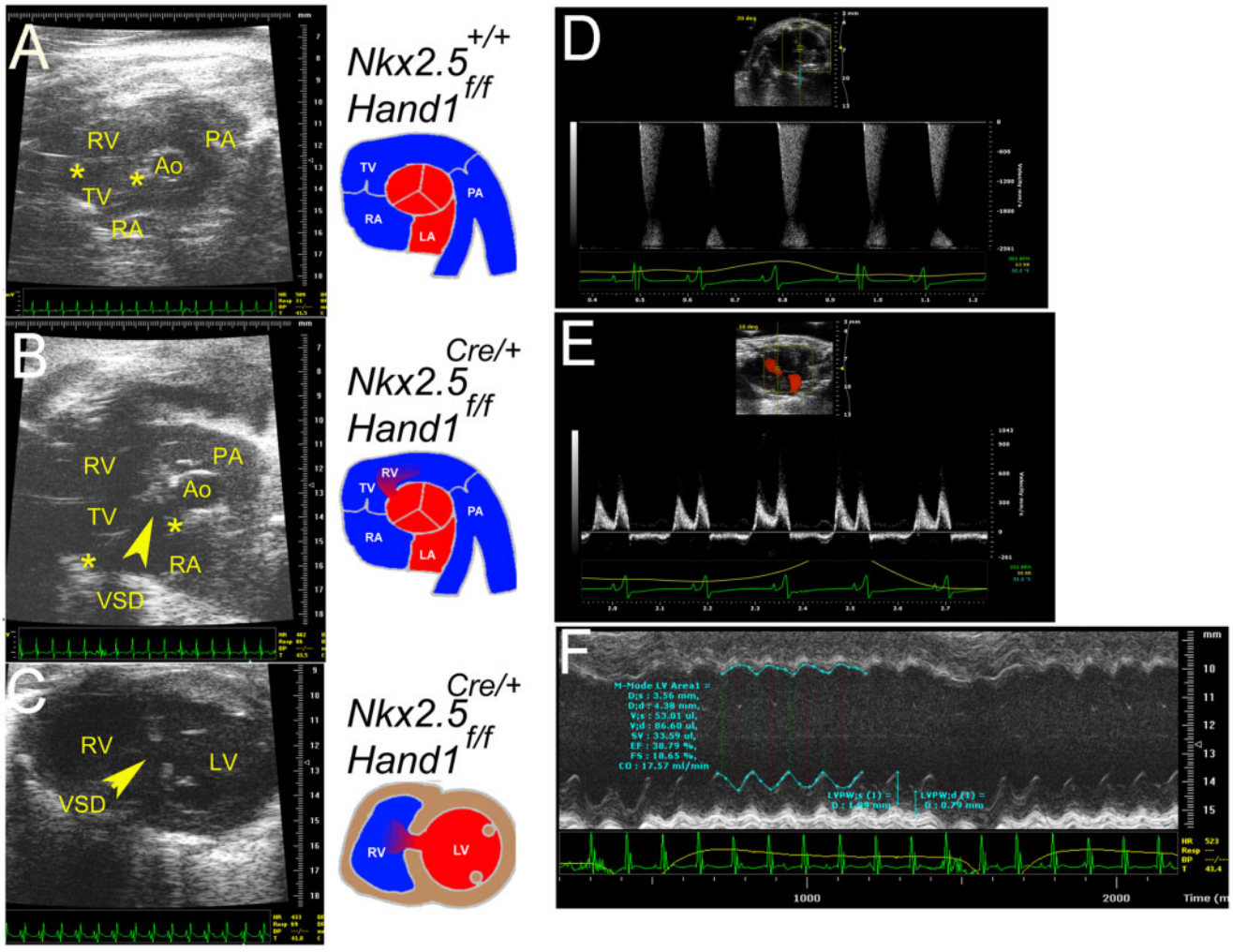

Figure 6 Documentation of cardiac defects living *Nkx2.5*$^{Cre/+}$;*Hand1*$^{f/f}$ mutant hearts via cardiac ultrasound. (*A*) Still, image with schematic drawing to the right representing a patent cardiac outflow tract in *Hand1*$^{f/f}$ control heart. (*B*) Image from a similar location as shown in A of *Nkx2.5*$^{Cre/+}$;*Hand1*$^{f/f}$ mutant that displays a membranous VSD (yellow arrowhead). (*C*) Still, image from a deeper plane showing a muscular VSD (yellow arrowhead) in a second *Nkx2.5*$^{Cre/+}$;*Hand1*$^{f/f}$ mutant. (*D*) Pulse wave Doppler evaluation of a high-velocity blood jet from a membranous VSD measured from the mouse in Supplementary material online, *Movie S1*. (*E*) Example of EA reversal in a *Nkx2.5*$^{Cre/+}$;*Hand1*$^{f/f}$ mutant. (*F*) M-mode evaluation of systolic function in a $P \geq 120$ *Nkx2.5*$^{Cre/+}$;*Hand1*$^{f/f}$ mutant showing poor systolic function with EF of only 38.79% and fractional shortening of 18.65%. Ao, aorta; LV, left ventricle; PA, pulmonary artery; RA, right atria; RV, right ventricle; TV, tricuspid valve (leaflets marked by asterisk); VSD, ventricular septal defect. $N = 6$.

conduction (the QRS interval) is lengthened in *Nkx2.5*$^{Cre/+}$;*Hand1*$^{f/f}$ when compared with controls (*Figure 3*). Significant changes in QRS complex length are detected via ECG in all three leads and more rigorous optical mapping analysis reveals epicardial breakthrough anomalies that include single LV breakthroughs and double LV breakthroughs with no observable RV breakthroughs in *H1CKOs*. Although a low incidence of abnormal ventricular conduction is observed in both the *Hand1*$^{f/f}$ and *Nkx2.5*$^{Cre/+}$ controls (*Figure 3*; *Table 2*) all of the six *Nkx2.5*$^{Cre/+}$;*Hand1*$^{f/f}$ mutants display right bundle branch block. Given that we observe significant reductions in embryonic gene expression of *Mybpc1* associated with bradycardia in Zebrafish,[46] cardiac conduction potassium channel *Hcn4* and tight junction protein CONNEXIN40 (*Gja5*) in our transcriptome analysis a direct role for HAND1 in cardiac conduction formation is a formal possibility; although, we cannot rule out that the VSDs and PM defects observed influence the changes in ventricular conduction. Furthermore, an abnormal conduction system could also impact cardiac function facilitating cardiac hypertrophy leading to heart failure. As the morphological and functional phenotypes in *H1CKO* are complex, it is currently unclear which components of this phenotype are causative to the heart failure. Equally important to note is that it is possible that a low level of *Hand1*, below current thresholds of detection, is expressed within the adult heart and some components of the observed phenotype are caused by this persistent expression. In our hands and in published studies *Hand1* mRNA is not detectable in the heart past E14.5, nevertheless, the possibility of extremely low levels of *Hand1* expression and function within the adult would be needed to fully test this hypothesis. Future studies collecting neonatal conduction data, adult Hand1 cardiomyocyte knockout, may reveal greater insights. Alternatively, it is well-established in the clinic that a left-right shunt often results in an enlarged RV leading to right heart failure, and this in turn, can cause RBB block

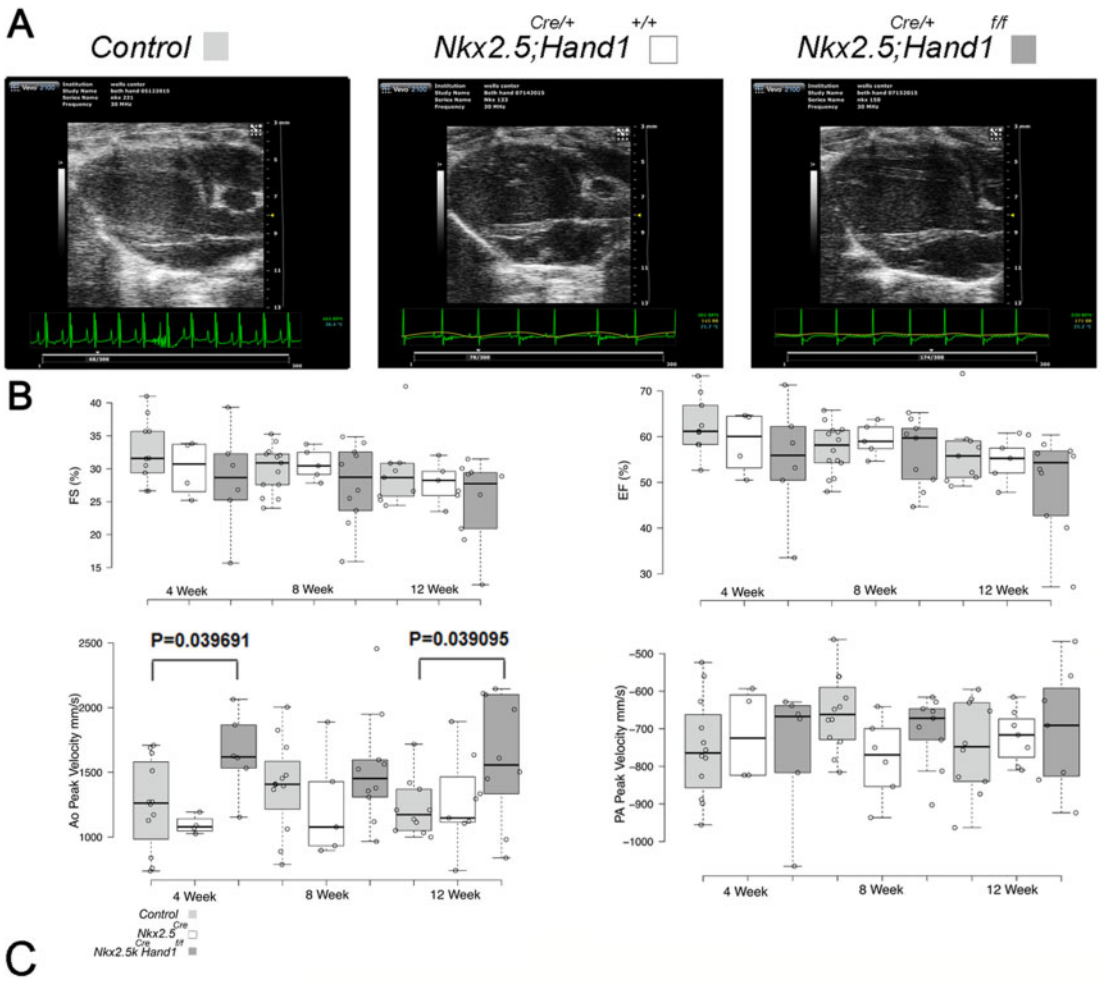

C

	Control	Nkx2.5;Hand1 Cre/+ f/f	Control	Nkx2.5;Hand1 Cre/+ f/f	Control	Nkx2.5;Hand1 Cre/+ f/f
	4 week		8 week		12 week	
A' (mm/s)	-18.66±5.29	-17.79±6.77	-19.85±7.58	-17.31±5.62	-17.72±5.97	-22.63±6.95
E' (mm/s)	-22.26±4.35	-21.44±6.97	-21.94±6.46	-21.20±6.01	-23.15±4.90	-24.61±4.91
IVRT (ms)	21.79±3.57	20.45±3.09	20.02±2.10	18.63±2.45	22.56±4.12	18.85±4.15
MV A (mm/s)	451.21±118.93	571.08±130.80*	451.48±169.82	568.45±144.98	423.63±131.55	641.24±175.09
MV Decel (ms)	28.77±6.95	27.88±8.54	24.96±3.93	25.02±6.40	22.51±9.76	16.96±4.99*
MV E (mm/s)	620.39±124.37	778.05±104.86**	590.19±167.25	756.01±166.78*	556.07±129.02	836.98±205.61*
E'/A'	1.24±0.14	1.23±0.14	1.15±0.18	1.25±0.21	1.35±0.24	1.14±0.24
MV E/A	1.41±0.24	1.45±0.49	1.40±0.39	1.39±0.37	1.37±0.31	1.35±0.30
MV E/E'	-28.62±7.39	-38.94±11.55	-27.94±6.95	-37.64±0.32*	-24.37±4.28	-35.51±12.63*

Figure 7 Functional analysis of young *Nkx2.5*^{Cre}; *Hand1*$^{f/f}$ mice show normal systolic function but altered peak aortic velocity. (*A*) Representative echocardiography still images of *Hand1*$^{f/f}$ control ($n = 12$, light grey), *Nkx2.5*^{Cre} control ($n = 12$, open) and *Nkx2.5*^{Cre}; *Hand1*$^{f/f}$ ($n = 12$, dark grey). (*B*) FS and EF at 4, 8, and 12 weeks of age show no changes in systolic function in *Nkx2.5*^{Cre}; *Hand1*$^{f/f}$ compared to controls. Doppler echocardiography measurement of aortic peak velocity (Ao peak) is significantly elevated ($P = 0.04$; one-way ANOVA) in mutants at 4 weeks and 12 weeks compared to controls. PA peak velocity is not significantly altered in Nkx2.5^{Cre}; *Hand1*$^{f/f}$ mice. In the box-scatter plots centre lines indicate medians; box limits indicate the 25th and 75th percentiles; whiskers indicate the 1.5X the interquartile range from the box limits; dots show number of animals *Hand1*$^{f/f}$ control ($n = 12$, light grey), *Nkx2.5*^{Cre} control ($n = 12$, open) and *Nkx2.5*^{Cre}; *Hand1*$^{f/f}$ ($n = 12$, dark grey). (*C*) Tissue Doppler analysis of MV A at 4 weeks (asterisk) and MV E velocities at 4, 8, and 12 weeks are significantly elevated in Nkx2.5^{Cre}; *Hand1*$^{f/f}$ mice compared to controls. Calculation of the mitral valve *E*/e' ratio reveals that this measure of increased atrial filling pressure is also significantly higher in *Nkx2.5*$^{Cre/+}$;*Hand1*$^{f/f}$ mice. *$P \leq 0.05$ **$P \leq 0.01$ via one-way ANOVA determined statistical significance with a $P \leq 0.05$ confidence. *A*', peak velocity of diastolic mitral annular motion determined by pulse wave Doppler; *E*', peak velocity of early diastolic mitral annular motion determined by pulse wave Doppler; *E*'/*A*', the *E*' to A' ratio; IVRT, isovolumic relaxation time; MV A, peak velocity of late transmitral flow; MV Decel, deceleration time of early diastolic transmitral flow; MV E, peak velocity of early diastolic transmitral flow; MV *E*/*A*, ratio of MV *E*/*A*; MV *E*/*E*', ratio of MV *E*/*E*'. ± indicates standard deviation. *Hand1*$^{f/f}$ control ($n = 12$, light grey), *Nkx2.5*^{Cre} control ($n = 12$, open), and *Nkx2.5*^{Cre}; *Hand1*$^{f/f}$ ($n = 12$, dark grey).

independently of cardiac conduction defects.[67] We cannot determine the causation of the RBB without further study.

Transcriptome analysis from E11.5 ventricles confirms the loss of *Hand1* as well as expected changes in gene expression in Hand1 downstream targets (see Supplementary material online, Data excel spread sheet *FIRULLI RNA SEQ Analysis* all results; *Figure 1*). *Hand1* is maximally expressed at E10.5 within the heart and E11.5 is the best window to look at the consequences of Hand1 cardiomyocyte loss-of-function. IPA determined that 28 biofunction categories hold a *Z* score of ≤ -2 or ≥2 (*Table 1*). Among these pathways, a clear correlation with the observed phenotypes of *H1CKOs* can be noted. Role of Nfat in cardiac hypertrophy; Cardiac hypertrophy signalling; Cardiac β-adrenergic signalling; and Renin–Angiotensin signalling are all associated pathways with cardiac dysfunction. What is truly intriguing here is that these pathways are altered in the E11.5 embryonic heart well before the adult cardiac phenotypes that these pathways are attributed to. Indeed, the idea that adult heart disease can be traced back to congenital origins is certainly a hypothesis that needs to be explored further. For instance, PKA signalling has an important role in the modulation of cardiac homoeostasis; however, PKA is also an important regulator of hand factors themselves regulating bHLH dimerization choices.[54,68] Indeed, *Mapkapk3,* a PKA pathway gene, which we validated the significant decreased gene expression (*Figure 1L*), codes for a Kinase that directly interacts with and represses the activity of the bHLH transcription factor E47,[69] a well-established Hand1 dimer partner. The greatest biofunction pathway change identified is Eif2 signalling with a *Z* sore of 5 (*Table 1*). To our surprise many of the regulated genes in this IPA class are ribosomal genes that are essential in facilitating protein translation. Upon further consideration, in order to increase the size of the heart, at least one of two mechanisms is required, either cardiomyocyte proliferation or cardiac hypertrophy, and both mechanisms rely on increased protein translation. As with the up-regulation of the hypertrophy-related pathways, the up-regulation of translation-related gene expression to support the hypertrophic growth in the E11.5 heart could be an indicator that many heart diseases associated with adult onset may have congenital origins in altered gene expression setting the stage for the manifestation of phenotype and pathology later in life. Our future plans are to look at this gene regulatory network in more detail and at earlier and later developmental time points to determine if Hand1 (associated with the transcriptional activation of RNA polymerase II-mediated gene expression) is also regulating genes associated with RNA polymerase I and or III (i.e. ribosomal subunits) and define HAND1 occupancy across the genome to refine searches for novel Hand1 transcriptional targets during cardiogenesis.

Supplementary material

Supplementary material is available at *Cardiovascular Research* online.

Acknowledgements

We thank Danny Carney and James N. O'Kane for technical assistance and Jeffery Tobin for helpful discussions. We thank all the researchers that shared reagents. We thank the Riley Heart Research Center for helpful discussions. Infrastructural support at the Herman B Wells Center for Pediatric Research, Riley Children's Foundation, and the Carrolton Buehl McCulloch Chair of Pediatrics.

Conflict of interest: none declared.

Funding

Infrastructural support at the Herman B Wells Center for Pediatric Research is in part supported by the generosity of the Riley Children's Foundation, Division of Pediatric Cardiology, and the Carrolton Buehl McCulloch Chair of Pediatrics. This work was supported by the National Institutes of Health [P01 HL134599-01, R01 HL145060-01, R01 HL122123-04, and R01 HL120920-04].

References

1. Olson EN. Gene regulatory networks in the evolution and development of the heart. *Science* 2006;**313**:1922–1927.
2. Pierpont ME, Basson CT, Benson DW Jr, Gelb BD, Giglia TM, Goldmuntz E, McGee G, Sable CA, Srivastava D, Webb CL; American Heart Association Congenital Cardiac Defects Committee; Council on Cardiovascular Disease in the Young. Genetic basis for congenital heart defects: current knowledge: a scientific statement from the American Heart Association Congenital Cardiac Defects Committee, Council on Cardiovascular Disease in the Young: endorsed by the American Academy of Pediatrics. *Circulation* 2007;**115**:3015–3038.
3. Gittenberger-de Groot AC, Blom NM, Aoyama N, Sucov H, Wenink AC, Poelmann RE. The role of neural crest and epicardium-derived cells in conduction system formation. *Novartis Found Symp* 2008;**250**:125–134. discussion 134-141.
4. Scholl AM, Kirby ML. Signals controlling neural crest contributions to the heart. *Wires Syst Biol Med* 2009;**1**:220–227.
5. Rochais F, Mesbah K, Kelly RG. Signaling pathways controlling second heart field development. *Circ Res* 2009;**104**:933–942.
6. Combs MD, Yutzey KE. Heart valve development: regulatory networks in development and disease. *Circ Res* 2009;**105**:408–421.
7. Porrello ER, Olson EN. Building a new heart from old parts: stem cell turnover in the aging heart. *Circ Res* 2010;**107**:1292–1294.
8. Gittenberger-de Groot AC, Winter EM, Poelmann RE. Epicardium-derived cells (EPDCs) in development, cardiac disease and repair of ischemia. *J Cell Mol Med* 2010;**14**:1056–1060.
9. Hoffman JI. Incidence of congenital heart disease: II. Prenatal incidence. *Pediatr Cardiol* 1995;**16**: 155–165.
10. Hoffman JI, Kaplan S, Liberthson RR. Prevalence of congenital heart disease. *Am Heart J* 2004;**147**:425–439.
11. Hinton RB, Martin LJ, Tabangin ME, Mazwi ML, Cripe LH, Benson W. Hypoplastic left heart syndrome is heritable. *J Am Coll Cardiol* 2007;**50**:1590–1597.
12. Webb GD, Smallhorn JF, Therrien J, Redington AN. *Congenital Heart Disease*. Philadelphia: Elsevier; 2011.
13. Hickey EJ, Caldarone CA, McCrindle BW. Left ventricular hypoplasia. *J Am Coll Cardiol* 2012;**59**:S43–S54.
14. Mori AD, Bruneau BG. TBX5 mutations and congenital heart disease: Holt-Oram syndrome revealed. *Curr Opin Cardiol* 2004;**19**:211–215.
15. Granados-Riveron JT, Pope M, Bu'lock FA, Thornborough C, Eason J, Setchfield K, Ketley A, Kirk EP, Fatkin D, Feneley MP, Harvey RP, Brook JD. Combined mutation screening of NKX2-5, GATA4, and TBX5 in congenital heart disease: multiple heterozygosity and novel mutations. *Congenit* 2012;**7**:151–159.
16. Wang J, Liu XY, Yang YQ. Novel NKX2-5 mutations responsible for congenital heart disease. *Genet Mol Res* 2011;**10**:2905–2915.
17. Nemer G, Fadlalah F, Usta J, Nemer M, Dbaibo G, Obeid M, Bitar F. A novel mutation in the GATA4 gene in patients with tetralogy of Fallot. *Hum Mutat* 2006;**27**:293–294.
18. Misra C, Sachan N, McNally CR, Koenig SN, Nichols HA, Guggilam A, Lucchesi PA, Pu WT, Srivastava D, Garg V. Congenital heart disease-causing Gata4 mutation displays functional deficits *in vivo*. *PLoS Genet* 2012;**8**:e1002690.
19. Cowan JR, Ware SM. Genetics and genetic testing in congenital heart disease. *Clin Perinatol* 2015;**42**:373–393, ix.
20. Riley P, Anson-Cartwright L, Cross JC. The Hand1 bHLH transcription factor is essential for placentation and cardiac morphogenesis. *Nat Genet* 1998;**18**:271–275.
21. Firulli AB, McFadden DG, Lin Q, Srivastava D, Olson EN. Heart and extra-embryonic mesodermal defects in mouse embryos lacking the bHLH transcription factor Hand1. *Nat Genet* 1998;**18**:266–270.
22. Firulli B, McConville DP, Byers JS, Vincentz JW, Barnes RM, Firulli AB. Analysis of a Hand1 hypomorphic allele reveals a critical threshold for embryonic viability. *Dev Dyn* 2010;**239**:2748–2760.
23. McFadden DG, Barbosa AC, Richardson JA, Schneider MD, Srivastava D, Olson EN. The Hand1 and Hand2 transcription factors regulate expansion of the embryonic cardiac ventricles in a gene dosage-dependent manner. *Development* 2004;**132**:189–201.
24. Reamon-Buettner SM, Ciribilli Y, Traverso I, Kuhls B, Inga A, Borlak J. A functional genetic study identifies HAND1 mutations in septation defects of the human heart. *Hum Mol Genet* 2009;**18**:3567–3578.
25. Reamon-Buettner SM, Ciribilli Y, Inga A, Borlak J. A loss-of-function mutation in the binding domain of HAND1 predicts hypoplasia of the human hearts. *Hum Mol Genet* 2008;**17**:1397–1405.

26. Esposito G, Butler TL, Blue GM, Cole AD, Sholler GF, Kirk EP, Grossfeld P, Perryman BM, Harvey R, Winlaw DS. Somatic mutations in NKX2–5, GATA4, and HAND1 are not a common cause of tetralogy of Fallot or hypoplastic left heart. *Am J Med Genet* 2011;**155**:2416–2421.
27. Cheng Z, Lib L, Li Z, Liu M, Yan J, Wang B, Ma X. Two novel HAND1 mutations in Chinese patients with ventricular septal defect. *Clin Chim Acta* 2012;**413**:675–677.
28. Zhou Y, Dai X, Qiu X, Yuan F, Li R, Xu Y, Qu X, Huang R, Xue S, Yang Y. HAND1 loss-of-function mutation associated with familial dilated cardiomyopathy. *Clin Chem Lab Med* 2015;**53**:1437–4331.
29. Firulli BA, Toolan KP, Harkin J, Millar H, Pineda S, Firulli AB. The HAND1 frameshift A126FS mutation does not cause hypoplastic left heart syndrome in mice. *Cardiovasc Res* 2017;**113**:1732.
30. Vincentz JW, Toolan KP, Zhang W, Firulli AB. Hand factor ablation causes defective left ventricular chamber development and compromised adult cardiac function. *PLoS Genet* 2017;**13**:e1006922.
31. Firulli BA, Fuchs RK, Vincentz JW, Clouthier DE, Firulli AB. Hand1 phosphoregulation within the distal arch neural crest is essential for craniofacial morphogenesis. *Development* 2014;**141**:3050–3061.
32. Firulli BA, Milliar H, Toolan KP, Harkin J, Fuchs RK, Robling AG, Firulli AB. Defective Hand1 phosphoregulation uncovers essential roles for Hand1 in limb morphogenesis. *Development* 2017;**144**:2480.
33. Moses KA, DeMayo F, Braun RM, Reecy JL, Schwartz RJ. Embryonic expression of an Nkx2-5/Cre gene using ROSA26 reporter mice. *Genesis* 2001;**31**:176–180.
34. Agah R, Frenkel PA, French BA, Michael LH, Overbeek PA, Schneider MD. Gene recombination in postmitotic cells. Targeted expression of Cre recombinase provokes cardiac-restricted, site-specific rearrangement in adult ventricular muscle *in vivo*. *J Clin Invest* 1997;**100**:169–179.
35. Dobin A, Davis CA, Schlesinger F, Drenkow J, Zaleski C, Jha S, Batut P, Chaisson M, Gingeras TR. STAR: ultrafast universal RNA-seq aligner. *Bioinformatics* 2013;**29**: 15–21.
36. Liao Y, Smyth GK, Shi W. featureCounts: an efficient general purpose program for assigning sequence reads to genomic features. *Bioinformatics* 2014;**30**:923–930.
37. Robinson MD, McCarthy DJ, Smyth GK. edgeR: a Bioconductor package for differential expression analysis of digital gene expression data. *Bioinformatics* 2010;**26**: 139–140.
38. McCarthy DJ, Chen Y, Smyth GK. Differential expression analysis of multifactor RNA-Seq experiments with respect to biological variation. *Nucleic Acids Res* 2012;**40**: 4288–4297.
39. Chen H, Zhang W, Li D, Cordes TM, Mark Payne R, Shou W. Analysis of ventricular hypertrabeculation and noncompaction using genetically engineered mouse models. *Pediatr Cardiol* 2009;**30**:626–634.
40. Zhu W, Shou W, Payne RM, Caldwell R, Field LJ. A mouse model for juvenile doxorubicin-induced cardiac dysfunction. *Pediatr Res* 2008;**64**:488–494.
41. Zhu W, Hassink RJ, Rubart M, Field LJ. Cell-cycle-based strategies to drive myocardial repair. *Pediatr Cardiol* 2009;**30**:710–715.
42. Mitchell GF, Jeron A, Koren G. Measurement of heart rate and Q-T interval in the conscious mouse. *Am J Physiol* 1998;**274**:H47–H51.
43. Maruyama M, Li B-Y, Chen H, Xu X, Song L-S, Guatimosim S, Zhu W, Yong W, Zhang W, Bu G, Lin S-F, Fishbein MC, Lederer WJ, Schild JH, Field LJ, Rubart M, Chen P-S, Shou W. FKBP12 is a critical regulator of the heart rhythm and the cardiac voltage-gated sodium current in mice. *Circ Res* 2011;**108**:1042–1052.
44. Cross JC, Flannery ML, Blanar MA, Steingrimsson E, Jenkins NA, Copeland NG, Rutter WJ, Werb Z. Hxt encodes a basic helix-loop-helix transcription factor that regulates trophoblast cell development. *Development* 1995;**121**: 2513–2523.
45. Ye F, Yuan F, Li X, Cooper N, Tinney JP, Keller BB. Gene expression profiles in engineered cardiac tissues respond to mechanical loading and inhibition of tyrosine kinases. *Physiol Rep* 2013;**1**:e00078.
46. Ha K, Buchan JG, Alvarado DM, McCall K, Vydyanath A, Luther PK, Goldsmith MI, Dobbs MB, Gurnett CA. MYBPC1 mutations impair skeletal muscle function in zebrafish models of arthrogryposis. *Hum Mol Genet* 2013;**22**:4967–4977.
47. Iruretagoyena JI, Davis W, Bird C, Olsen J, Radue R, Teo Broman A, Kendziorski C, Splinter BonDurant S, Golos T, Bird I, Shah D. Metabolic gene profile in early human fetal heart development. *Mol Hum Reprod* 2014;**20**:690–700.
48. Milano A, Vermeer AM, Lodder EM, Barc J, Verkerk AO, Postma AV, van der Bilt IA, Baars MJ, van Haelst PL, Caliskan K, Hoedemaekers YM, Le Scouarnec S, Redon R, Pinto YM, Christiaans I, Wilde AA, Bezzina CR. HCN4 mutations in multiple families with bradycardia and left ventricular noncompaction cardiomyopathy. *J Am Coll Cardiol* 2014;**64**:745–756.
49. van Weerd JH, Christoffels VM. The formation and function of the cardiac conduction system. *Development* 2016;**143**:197–210.
50. Kim YS, Jung SH, Jung DH, Choi SJ, Lee YR, Kim JS. Gas6 stimulates angiogenesis of human retinal endothelial cells and of zebrafish embryos via ERK1/2 signaling. *PLoS One* 2014;**9**:e83901.
51. Rees WD, Hay SM, Fontanier-Razzaq NC, Antipatis C, Harries DN. Expression of the growth arrest genes (GAS and GADD) changes during organogenesis in the rat fetus. *J Nutr* 1999;**129**:1532–1536.
52. Cavallero S, Shen H, Yi C, Lien CL, Kumar SR, Sucov HM. CXCL12 signaling is essential for maturation of the ventricular coronary endothelial plexus and establishment of functional coronary circulation. *Dev Cell* 2015;**33**:469–477.
53. Harrison MR, Bussmann J, Huang Y, Zhao L, Osorio A, Burns CG, Burns CE, Sucov HM, Siekmann AF, Lien CL. Chemokine-guided angiogenesis directs coronary vasculature formation in zebrafish. *Dev Cell* 2015;**33**:442–454.
54. Firulli B, Howard MJ, McDaid JR, McIlreavey L, Dionne KM, Centonze V, Cserjesi P, Virshup DMa, Firulli AB. PKA, PKC and the protein phosphatase 2A influence HAND factor function: a mechanisms for tissue specific transcriptional regulation. *Mol Cell* 2003;**12**:1225–1237.
55. Lu G, Ota A, Ren S, Franklin S, Rau CD, Ping P, Lane TF, Zhou ZH, Reue K, Lusis AJ, Vondriska T, Wang Y. PPM1l encodes an inositol requiring-protein 1 (IRE1) specific phosphatase that regulates the functional outcome of the ER stress response. *Mol Metab* 2013;**2**:405–416.
56. Barnes RM, Firulli B, Conway SJ, Vincentz JW, Firulli AB. Analysis of the Hand1 cell lineage reveals novel contributions to cardiovascular, neural crest, extra-embryonic, and lateral mesoderm derivatives. *Dev Dyn* 2010;**239**:3086–3097.
57. Barnes RM, Firulli BA, VanDusen NJ, Morikawa Y, Conway SJ, Cserjesi P, Vincentz JW, Firulli AB. Hand2 loss-of-function in Hand1-expressing cells reveals distinct roles in epicardial and coronary vessel development. *Circ Res* 2011;**108**:940–949.
58. Losada E, Moon-Grady AJ, Strohsnitter WC, Wu D, Ursell PC. Anomalous mitral arcade in twin-twin transfusion syndrome. *Circulation* 2010;**122**:1456–1463.
59. Marino BS, Kruge LE, Cho CJ, Tomlinson RS, Shera D, Weinberg PM, Gaynor JW, Rychik J. Parachute mitral valve: morphologic descriptors, associated lesions, and outcomes after biventricular repair. *J Thorac Cardiovasc Surg* 2009;**137**:385–393.e384.
60. Biben C, Harvey RP. Homeodomain factor Nkx2-5 controls left/right asymmetric expression of bHLH gene eHand during murine heart development. *Genes Dev* 1997; **11**:1357–1369.
61. Layman TE, Edwards JE. Anomalous mitral arcade. *Circulation* 1967;**35**:389–395.
62. Parr GVS, Fripp RR, Whitman V, Bharati S, Lev M. Anomalous mirtal arcade: ecocardoigraphic and angiographic recognition. *Pediatr Cardiol* 1983;**4**:163–165.
63. Braunwald E, Awe WC. The syndrome of severe mitral regurgitation with normal left atrial pressure. *Circulation* 1963;**27**:29–35.
64. Collins RT 2nd, Ryan M, Gleason MM. Images in cardiovascular medicine. Mitral arcade: a rare cause of fatigue in an 18-year-old female. *Circulation* 2010;**121**: e379–e383.
65. Lekavich CL, Barksdale DJ, Neelon V, Wu J. Heart failure preserved ejection fraction (HFpEF): an integrated and strategic review. *Heart Fail Rev* 2015;**20**:643–653.
66. Grifka RG, O'Laughlin MP, Nihill MR, Mullins CE. Double-transseptal, double balloon valvuloplasty for congenital mirtal stenosis. *Circulation* 1992;**85**:123–129.
67. Kastor JA, Goldreyer BN, Moore NE, Shelburne JC, Manchester JH. Intraventricular conduction in man studied with an endocardial electrode catheter mapping technique. Patients with normal QRS and right bundle branch block. *Circulation* 1975;**51**: 786–796.
68. Vincentz JW, Barnes RM, Firulli AB. Hand factors as regulators of cardiac morphogenesis and implications for congenital heart defects. *Birth Defects Res A Clin Mol Teratol* 2011;**91**:485–494.
69. Neufeld B, Grosse-Wilde A, Hoffmeyer A, Jordan BW, Chen P, Dinev D, Ludwig S, Rapp UR. Serine/Threonine kinases 3pK and MAPK-activated protein kinase 2 interact with the basic helix-loop-helix transcription factor E47 and repress its transcriptional activity. *J Biol Chem* 2000;**275**:20239–20242.

Translational perspective

Cardiogenesis is a complex process that integrates the cell specification and morphological patterning of a number of cell types to form a patent functioning heart. The bHLH factor HAND1 is expressed within the early heart left ventricular myocardium where its loss of function impacts left ventricular morphology and mitral valve function. Moreover, cardiac conduction is altered in *Hand1* mutant mice resembling right bundle branch block. Clinically, this data suggest that examining mutations in *HAND1* in adults may prove an effective marker for cardiac disease.